www.czasopisma.pan.pl PAN POLSKA AKADEMIA NAUK www.journals.pan.pl

Arch. Metall. Mater., Vol. 61 (2016), No 3, p. 1529–1536

DOI: 10.1515/amm-2016-0250

M. WROŃSKI*, K. WIERZBANOWSKI*,#

LATTICE ROTATION DEFINITION AND PREDICTED TEXTURES OF TENSILE AND COMPRESSION DEFORMATION

Abstract. The problem of ambiguity in the definition of lattice rotation, used in plastic deformation models, is examined in this work. The geometry of tensile and compression deformation is considered. Two approaches to lattice rotation are considered: the classical definition (called also 'mathematical analysis') and the definition based on orientation preservation of specified directions/planes in the sample coordinates system. Similar study was already done by the present authors for the geometry of rolling deformation. It was shown that application of two rotation definitions enables to explain the appearance of two types of f.c.c. rolling textures: brass type and copper type textures. In the case of axisymmetric deformation the application of both definitions of lattice rotation leads to similar textures, but with different spread of their principal components.

Keywords: axisymmetric deformation, texture, lattice rotation, deformation models

1. Introduction

The definition of lattice rotation is an important issue in plastic deformation models. This problem originated from the work of Hosford [1] and it was correctly defined and examined in [2,3]. It was thoroughly studied in the case of rolling deformation in the last years [4-8]. Let us recall an example concerning rolling process geometry. Two possible lattice rotations of a deformed grain are illustrated in Fig. 1. An initially cubic grain is presented in two dimensional projection and its deformation, caused by a shear on the marked slip system with ***m*** slip direction and ***n*** slip plane, is shown in Fig. 1a. In the presented example x_1 is parallel to the rolling direction (RD) and x_3 is parallel to the normal direction (ND); the x_2 axis, perpendicular to the plane of figure, is parallel to the transverse direction (TD). The resulting shape of this grain after occurrence of simple slip is shown in Fig. 1b. Till this stage the crystal lattice did not change its orientation. Each polycrystalline grain interacts, however, with its environment and some rigid body rotation is imposed. When classical rotation definition (CL definition) is applied (see section 2.2.1) the grain has a final position as sketched in Fig. 1c. Another definition of rotation is based on the orientation preservation (PR definition) of specified planes and directions in the sample coordinates frame. In the example shown in Fig. 1d a material plate parallel to rolling plane (RD,TD) and of a string of material parallel to rolling direction (RD) preserve their orientation in the sample coordinates frame. This condition results directly from the rolling deformation geometry. It is obvious that resulting final orientations of the crystal lattice are different in two presented cases.

Application of these two definitions of crystal lattice rotation and of different magnitudes of interaction between a grain and its environment (L parameter; see Section 2.1) leads to very good predictions of two types of f.c.c. rolling textures, i.e., brass and copper types - Fig.2. This problem was widely discussed in [6] and [8], where it was argued that deformation and textures of low stacking fault energy metals (e.g., brass, silver) are correctly described, when low values of interaction parameter (L) are used. In contrast, higher values of L should be used in the case of high stacking fault energy metals (e.g., copper). The model predicted textures of Fig.2 agree well with experimental ones, in spite of higher intensities of the predicted textures, which is a typical effect. The existence of two types of f.c.c. rolling textures was the subject of a long discussion in the literature [9-17].

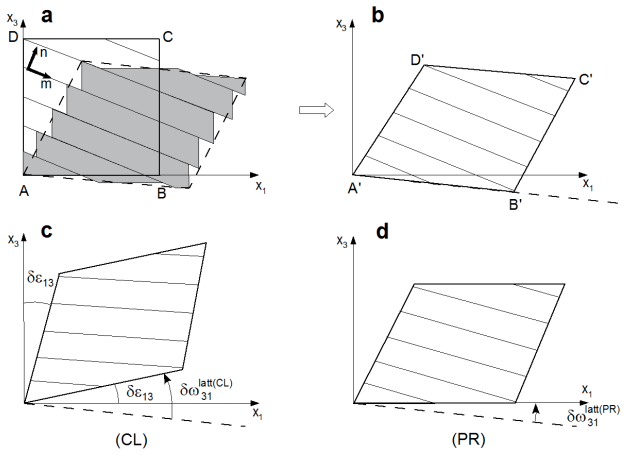

Fig. 1. Deformation of an initially cubic sample seen in two-dimensional projection: a) shear occurred on the slip system (***n, m***), b) shape and position of the grain (A'B'C'D') after slip only, c) position after slip and CL lattice rotation, d) position after slip and PR lattice rotation [8]

* AGH UNIVERSITY OF SCIENCE AND TECHNOLOGY, FACULTY OF PHYSICS AND APPLIED COMPUTER SCIENCE, AL. MICKIEWICZA 30, 30-059 KRAKÓW, POLAND

Corresponding author: wierzbanowski@fis.agh.edu.pl

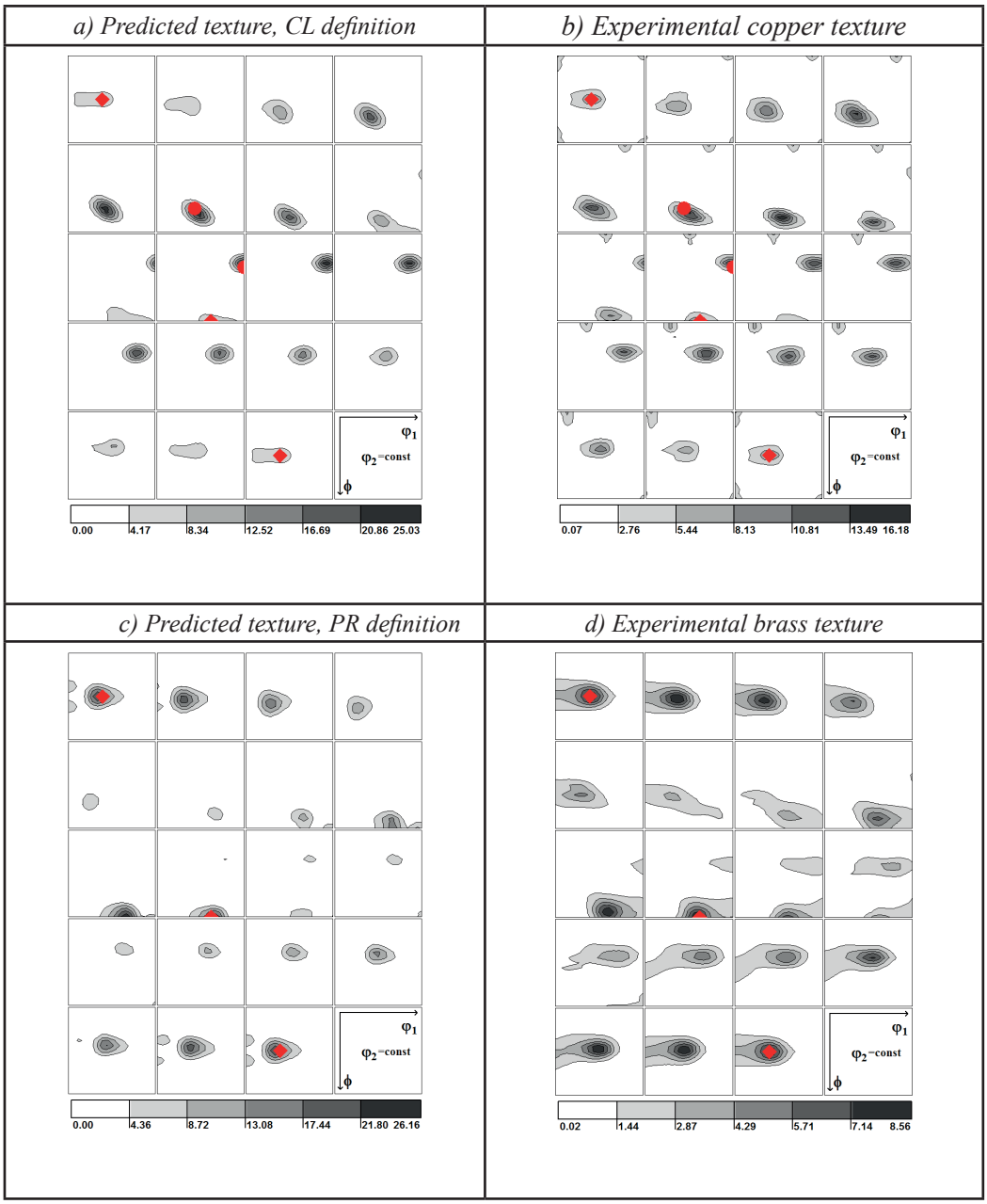

Fig. 2. Predicted and calculated ODFs: a) simulated with CL definition of lattice rotation, <110>{111} slip, L=800 MPa, b) experimental ODF of polycrystalline copper; C (●) - copper orientation and B (♦) - brass orientation are marked, c) simulated with PR lattice rotation definition, <110>{111} slip, L=100 MPa, d) experimental ODF of polycrystalline brass ; B (♦) - brass orientation is marked. Rolling reduction for calculated and experimental textures is 50%

2. Deformation model

2.1. Short description of crystallographic deformation model

Each crystallographic deformation model contains two basic elements:

- law of interaction between crystallites and their environment,
- description of deformation mechanisms on crystal level.

The interaction between a grain and an average material (matrix) is described in the used model by the following law [18,19]:

$$\dot{\sigma}_{ij} = \dot{\Sigma}_{ij} + L(\dot{E}^{pl}_{ij} - \dot{\varepsilon}^{pl}_{ij}) \tag{1}$$

where σ_{ij} and ε^{pl}_{ij} are local stress and plastic strain of a grain, and Σ_{ij} and E^{pl}_{ij} are analogous quantities for the sample; dot denotes time derivative. The interaction magnitude between a grain and the sample is described by L parameter. For f.c.c. metals L is typically in the range between 0 (Sachs model) and 800 MPa (statistical Taylor model). In the present work the value L=800 MPa was used for the prediction of tensile and compression textures.

The basic deformation mechanism in f.c.c. and b.c.c metals is crystallographic slip. It occurs on slip planes *{hkl}* along slip directions <*uvw*> laying on these planes.

Accordingly, one defines slip system families: <*uvw*>{*hkl*}. The considered slip systems were <110>{111} ones for f.c.c. structure and <111>{110}, <111>{112} , <111>{123} for b.c.c. structure metals. A given slip system becomes active if the resolved shear stress τ, occurring on it, equals or exceeds the critical stress for slip τ_{cr} (Schmid law):

$$\tau \geq \tau_{cr} \tag{2}$$

The resolved stress on a slip system, defined by the unit vector ***m*** along slip direction and by the unit ***n*** vector perpendicular to the slip plane, is calculated as:

$$\tau = m_i n_j \sigma_{ij} \tag{3}$$

where m_i and n_j are components of ***m*** and ***n*** vectors; moreover, the convention of summation on repeated lower indices is applied in this work. The critical stresses for slip increase during deformation due to the work hardening. The linear hardening law was used, therefore an increase of τ_{cr} for the slip system *'i'* after a given calculation increment is:

$$\Delta\tau^i_{cr} = h\sum_j H^{ij}\delta\gamma^j \tag{4}$$

where H^{ij} is the hardening matrix, h is its amplitude, $\delta\gamma^j$ is the slip shear increment on the *j-th* slip system and summation is done for over all active slip systems. The simple form of the hardening matrix was used, i.e., $H^{ij}=1$ for $i=j$ and $H^{ij}=A$ for $i\neq j$. The A coefficient defines the type of hardening: $A=1$ is used for isotropic hardening (applied in this work) and $A>1$ for anisotropic hardening.

After a series of slip shears, the increase of the grain displacement gradient is:

$$\Delta e^{pl}_{ij} = \frac{1}{2}\sum_s m^s_i n^s_j \delta\gamma^s \tag{5}$$

and that of grain plastic strain:

$$\Delta\varepsilon^{pl}_{ij} = \frac{1}{2}\sum_s (m^s_i n^s_j + m^s_j n^s_i)\delta\gamma^s \tag{6}$$

where summation is done on all active slip systems (numbered by *s*). Finally, the sample strain is the average of grain strains:

$$E^{pl}_{ij} = <\varepsilon^{pl}_{ij}> = \frac{1}{V_0}\sum_I \varepsilon^{pl(I)}_{ij} V^I \tag{7}$$

where V^I is the volume of *I-th* grain, V_0 is the sample volume and summation is carried over all grains. And finally, what concerns the lattice rotation, it can be based on two definitions discussed in the next section.

2.2. Lattice rotation

A general relation defining the rotations appearing in deformation modeling is (see, e.g., [20]):

$$\delta\Omega_{ij} = \delta\Omega^{pl}_{ij} + \delta\Omega^{latt}_{ij} \tag{8}$$

where $\delta\Omega_{ij}$ is the increment of the total spin of the sample, $\delta\Omega^{pl}_{ij}$ is the increment of the plastic spin (produced by shears on active slip systems) and $\delta\Omega^{latt}_{ij}$ is the auxiliary rotation resulting from mechanical constraints imposed on the sample. Therefore:

$$\delta\Omega^{latt}_{ij} = \delta\Omega_{ij} - \delta\Omega^{pl}_{ij} \tag{9}$$

2.2.1 Classical definition (CL)

In some works the classical definition (*CL*) of lattice rotation is adopted. If one assumes no resultant rigid body rotation of the sample ($\delta\Omega_{ij}=0$) and of a grain ($\delta\omega_{ij}=0$), then a *grain* plastic rotation, $\delta\omega^{pl}_{ij}$, after every increment of the slip shear has to be compensated by an auxiliary grain lattice rotation $\delta\omega^{latt-CL}_{ij}$:

$$\delta\omega^{latt-CL}_{ij} = -\delta\omega^{pl}_{ij} = -\frac{1}{2}(m_i n_j - m_j n_i)\,\delta\gamma \tag{10}$$

A sum of these rotation increments occurring in a given calculation step, which results from shears on active slip systems (numbered by *s*), determines a final orientation change of a grain lattice:

$$\Delta\omega^{latt-CL}_{ij} = \sum_s \delta\omega^{latt-CL(s)}_{ij} \tag{11}$$

The CL definition is universal, i.e., it is applicable for any deformation geometry. It is used in some handbooks (e.g., [21]) and papers (e.g. [22]).

2.2.2 Definition based on preservation condition (PR)

Another approach is based on the assumption that specific sample planes/directions preserve constant orientations in the sample reference system (*PR* definition). Such the condition is imposed by a deformation geometry and let us consider that it is also fulfilled by each grain. In the case of rolling, where the orientation preservation of rolling direction (x_1 axis) direction and of rolling plane (x_1x_2 plane) is assumed, it leads to the compensation of the following components of the grain displacement gradient tensor: $\delta e^{pl}_{21} = m_2 n_1 \delta\gamma$, $\delta e^{pl}_{31} = m_3 n_1 \delta\gamma$ and $\delta e^{pl}_{32} = m_3 n_2 \delta\gamma$. This leads to the following grain lattice rotation, occurring after each slip shear increment δγ [4,8]:

$$\delta\omega^{latt-PR}_{ij} = \delta\gamma \begin{bmatrix} 0 & m_2 n_1 & m_3 n_1 \\ -m_2 n_1 & 0 & m_3 n_2 \\ -m_3 n_1 & -m_3 n_2 & 0 \end{bmatrix} \tag{12}$$

The total grain rotation, $\delta\omega_{ij} = \delta\omega^{latt-PR}_{ij} + \delta\omega^{pl}_{ij}$, after a shear increment is not equal to zero in this case, but its value is strongly reduced after a series of glides on different slip systems (multi-slip). The same concerns the sample rotation Ω_{ij}. The resulting rotation of grain lattice after a series of glides is:

$$\Delta\omega^{latt-PR}_{ij} = \sum_s \delta\omega^{latt-PR(s)}_{ij} \tag{13}$$

In the present work we examine, however, the case of

axisymmetric deformation, i.e., tensile and compression tests. Thus, in the case of *tensile test along* x_3 sample axis, a string of material parallel to this axis cannot be inclined towards axes x_1 and x_2. Consequently, δe_{13}^{pl} and δe_{23}^{pl} have to compensated by the lattice rotation:

$$\delta\omega_{ij}^{latt(PR)} = \delta\gamma \begin{bmatrix} 0 & 0 & -m_1 n_3 \\ 0 & 0 & -m_2 n_3 \\ m_1 n_3 & m_2 n_3 & 0 \end{bmatrix} \tag{14}$$

In the above equation $\delta\omega_{12}^{latt-PR} = -\delta\omega_{21}^{latt-PR} = 0$, because any specific relation between orientations of x_1 and x_2 sample axes is not imposed by the deformation geometry and an obvious relation is verified: $\delta\omega_{ij}^{latt-PR} = -\delta\omega_{ji}^{latt-PR}$.

The example of tensile deformation of a single crystal along x_3 axis and resulting lattice rotation is shown in Fig. 3.

In the case of the compression along x_3 direction a plate of material perpendicular to this direction, i.e., x_1x_2, plane has to preserve constant orientation. This leads to a requirement that the δe_{31}^{pl} and δe_{32}^{pl} components of the displacement gradient tensor have to be compensated by respective components of the lattice rotation tensor:

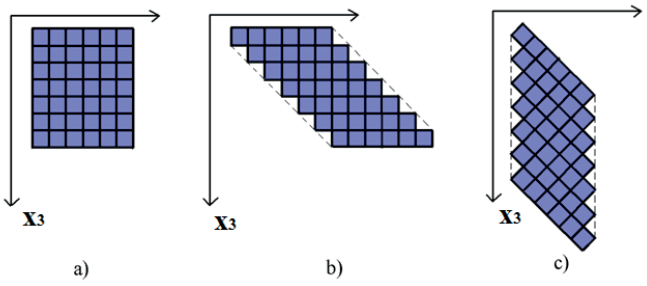

Fig. 3. Tensile deformation of a single crystal along x_3 axis: a) before slip, b) after slip, c) after slip and lattice rotation assuring constant orientation of a string of material parallel to the tensile axis (x_3 axis)

$$\delta\omega_{ij}^{latt-PR} = \delta\gamma \begin{bmatrix} 0 & 0 & m_3 n_1 \\ 0 & 0 & m_3 n_2 \\ -m_3 n_1 & -m_3 n_2 & 0 \end{bmatrix} \tag{15}$$

Here again, $\delta\omega_{12}^{latt-PR} = -\delta\omega_{21}^{latt-PR} = 0$, because any specific relation between orientations of x_1 and x_2 sample axes is not imposed by the deformation geometry and an obvious relation has to be verified: $\delta\omega_{ij}^{latt-PR} = -\delta\omega_{ji}^{latt-PR}$.

a) *Predicted pole figures, CL definition*

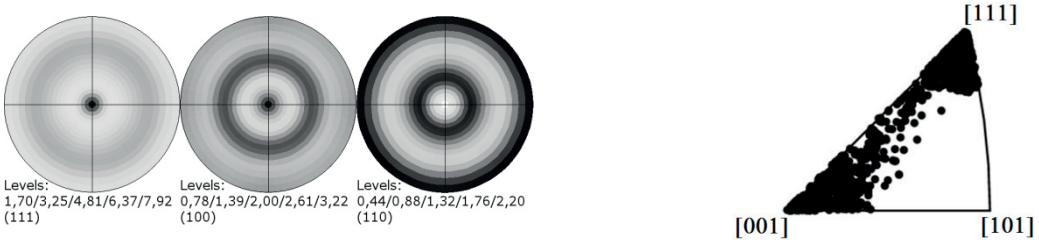

b) *Predicted pole figures, PR definition*

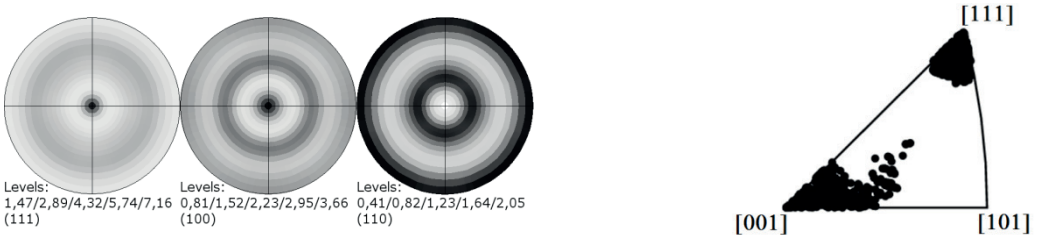

c) *Experimental*

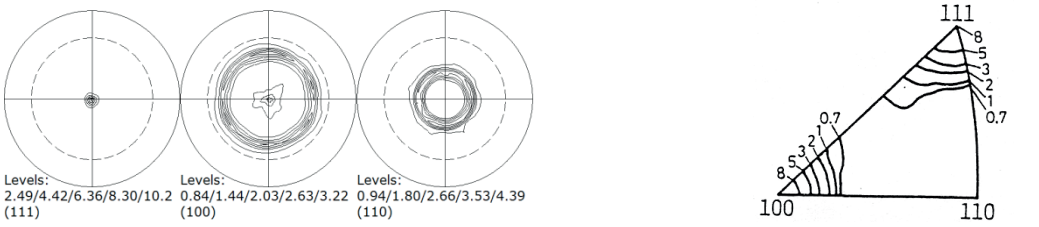

Fig.4 Tensile f.c.c. textures represented by {111}, {100}, {110} PFs and IPFs for tensile direction: a) predicted with CL definition, b) predicted with PR definition, c) experimental PFs for aluminum and IPF for copper [23])

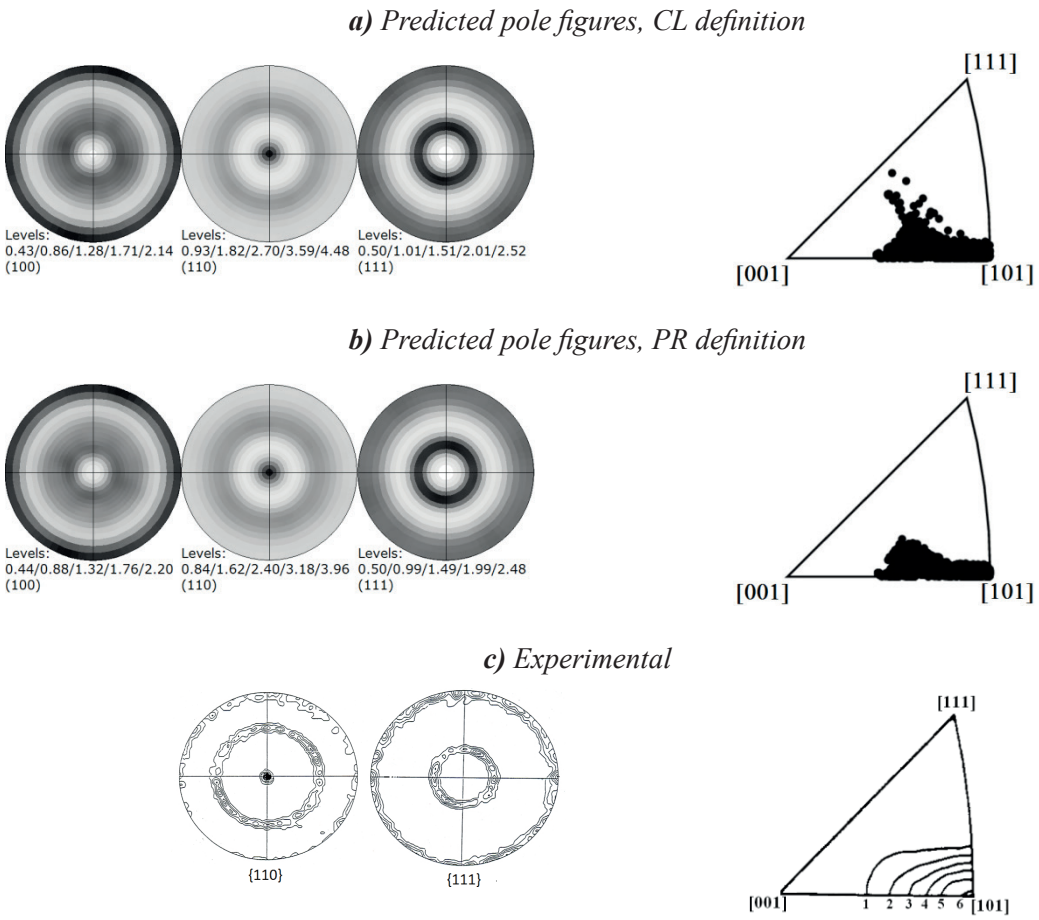

Fig. 5. Tensile b.c.c. textures represented by {111}, {100}, {110} PFs and IPFs for tensile direction: a) predicted with CL definition, b) predicted with PR definition, c) experimental PFs for tungsten [24]) and IPF for Fe wire [25]

3. Predicted textures of axisymmetric deformation

The calculations presented in this section concern medium and high stacking fault energy metals, therefore the value of L=800 MPa was used. *CL* and *PR* lattice rotation definitions were used and the final strain was ε=0.6. In the case of tensile and compression textures it is convenient to use pole figures (PFs) and inverse pole figures (IPFs) and they are analyzed in this section. The experimental data was taken from literature, except of PFs of aluminum from Fig.4c.

3.1. Tensile deformation, f.c.c. structure

Predicted and experimental PFs and IPFs for the stretched f.c.c. polycrystalline materials are shown in Fig.4. The predicted {100}, {110} and {111} PFs seem to be identical for *CL* and *PR* rotation definitions and they agree perfectly with maxima of experimental PFs for aluminum. However, subtle differences between predicted textures can be detected analyzing IPFs for tensile direction (x_3). Both model calculated textures contain <100> and <111> fiber components, which is in agreement with experimental texture. Nevertheless, when comparing IPFs from Figs.4a and 4b, one finds that *CL* texture contains an important spread of orientations between <100> and <111> fibers, which do not appear in experimental IPF (Fig. 4c). Therefore, PR definition gives a better texture prediction, closer to experimental data.

3.2. Tensile deformation, b.c.c. structure

Predicted and experimental PFs and IPFs for the stretched b.c.c. polycrystalline metals are shown in Fig.5. The predicted {100}, {110} and {111} PFs seem to be identical for *CL* and PR rotation definitions. A comparison with experimental {110} and {111} PFs of tungsten confirms a very good agreement. However, the IPF predicted with *CL* definition is more dispersed than that obtained with *PR* one. The latter is closer to the experimental IPF - Fig. 5c.

3.3. Compression deformation, f.c.c. structure

Both definitions lead to very similar textures, dominated by the <110> fiber component (Figs.6a,b). In addition one observes in IPF_s a "tail" of orientations, starting from <110> towards <100>, which is in a very good agreement with experiment (Fig.6c). However, as in the preceding cases, the

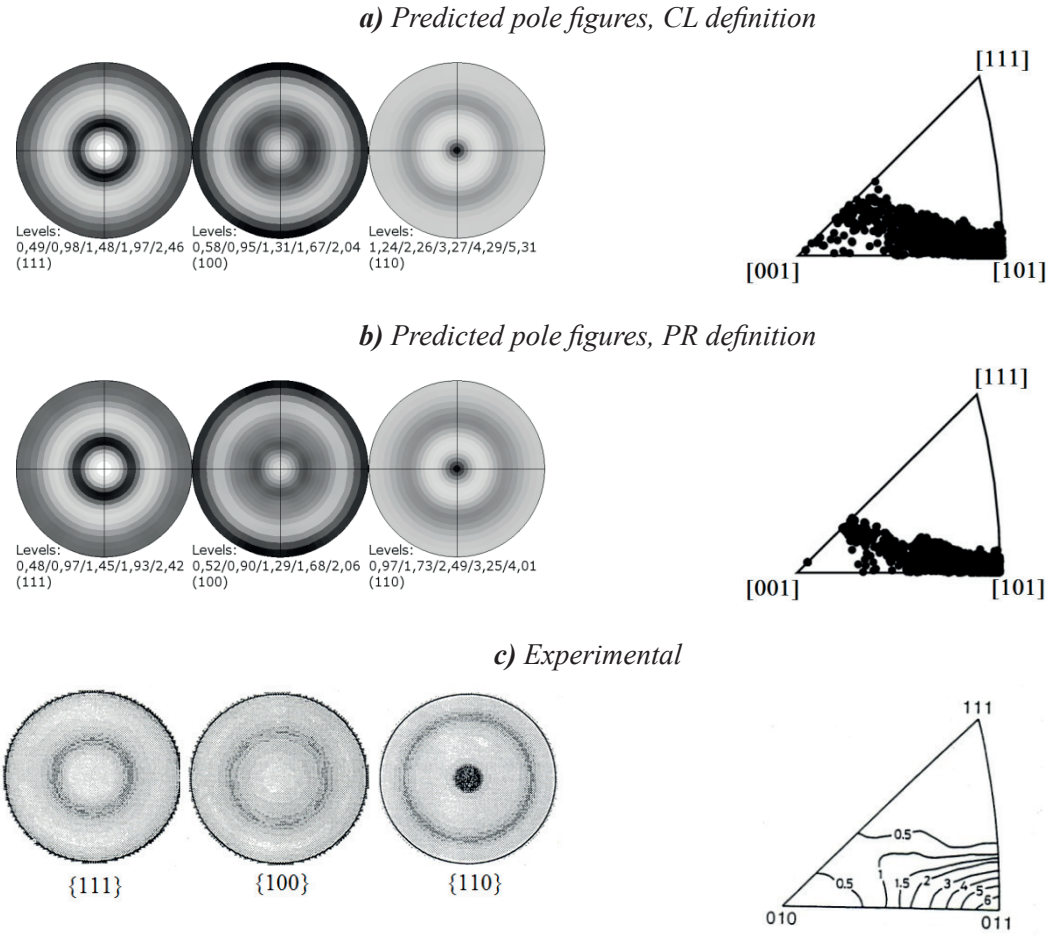

Fig.6. Compression f.c.c. textures represented by {111}, {100}, {110} PFs and IPFs for tensile direction:, a) predicted with CL definition, b) predicted with PR definition, c) experimental PFs for copper [26] and IFP for nickel [27]

predicted IFP is less dispersed in the case of *PR* definition than in the case of *CL*, which is closer to experimental IFP.

3.4. Compression deformation, b.c.c. structure

Predicted and experimental PFs and IPFs for compressed b.c.c. polycrystalline metals are shown in Fig.7. The predicted {100}, {110} and {211} PFs with *CL* and *PR* rotation definitions are very similar and they agree with experimental PFs for steel. However, some difference between *CL* and *PR* predicted textures are visible on IPFs. Both model calculated textures contain <100> and <111> fiber components, which is in agreement with experimental texture, but the *CL* texture contains also a spread of orientations between <100> and <111> fibers, which do not appear in experimental IPF (Fig. 7c). Therefore, PR definition gives a better texture prediction, closer to experimental data. This is analogous result to that of f.c.c. tensile texture (Fig. 4).

4. Conclusions

The examined two types of lattice rotation definition (*CL* and *PR*), used in the deformation model, lead to similar predicted textures of axisymmetric deformation for f.c.c. and b.c.c. polycrystalline metals, very close to experimental ones.

One can ask, why pole figures predicted with the two discussed lattice rotation definitions are so close. The reason is the occurrence of the multi-slip during plastic deformation. The relations given by Eqs.10,12,14 concern one elementary slip event with a small shear amplitude. However, the final plastic strain and a change of lattice orientation of each grain result from a series of consecutive slip events on different slip systems. This fact is expressed by Eqs. 5,6,11,13. The action of multi-slip process leads to averaging of lattice rotations produced by individual slip systems. This effect reduces the effect of different *CL* and *PR* definitions and correspondingly the predicted textures.

In spite of the above textures similarities, some differences between textures calculated using *CL* and *PR* lattice rotations can be pointed out. They consists in visibly wider dispersions of texture maxima in the case of *CL* definition. Our calculations show that textures obtained with *PR* definition are closer to the experimental data.

It can be noted, however, that differences between *CL* and *PR* calculated textures are less significant in the case of axisymmetric deformation than in the case of rolling process. This can be explained by a higher sensibility on the rotation definition in the case of lower symmetry deformation (i.e., rolling versus axisymmetric deformation).

a) Predicted pole figures, CL definition

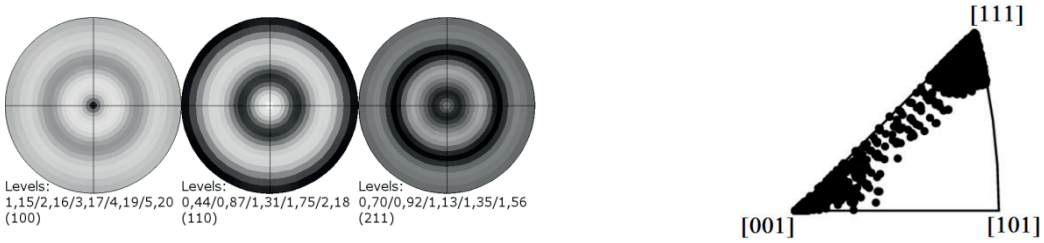

b) Predicted pole figures, PR definition

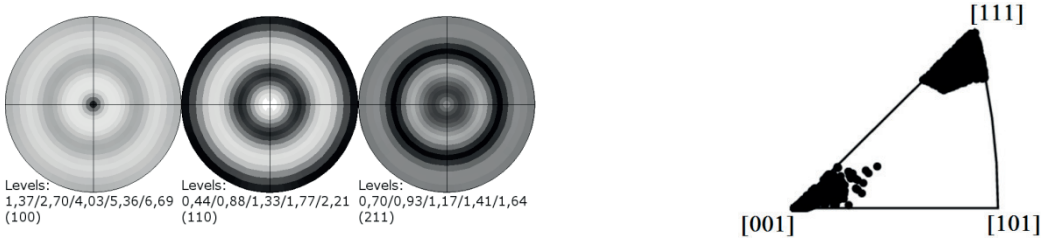

c) Experimental

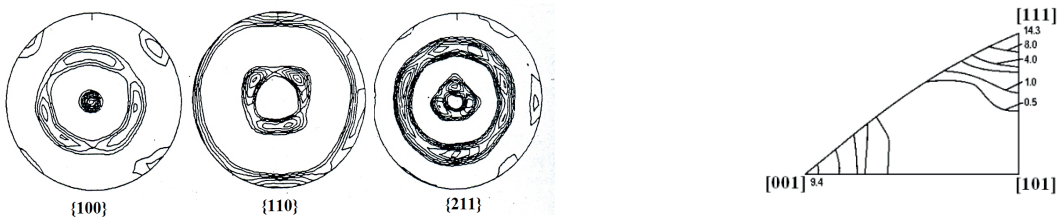

Fig. 7. Compression b.c.c. textures represented by {111}, {100}, {110} PFs and IPFs for tensile direction:, a) predicted with CL definition, b) predicted with PR definition, c) experimental PFs[28] and IPF [29] for steel

It can be also mentioned that deformation models are used for interpretation of the residual stress measurements by X-ray and neutron diffraction [30-32]. The use of *CL* or *PR* definitions of lattice rotation can modify the estimated residual stress values [33].

Acknowledgements

This work was supported by the National Science Centre (NCN) on the basis of decision DEC-2013/11/B/ST3/03787.

REFERENCES

[1] W.F. Hosford, Texture of Crystalline Solids **2**, 175-182 (1977).
[2] R.A. Lebensohn , T. Leffers, Texture Microstruct. **31**, 217-230 (1999).
[3] T. Leffers, R.A. Lebensohn, Proc. of the 11th. Int. Conf. on Textures of Materials (ICOTOM-11), Z. Liang et al. eds., International Academic Publ., pp. 307-314 (1996).
[4] K. Wierzbanowski, M. Wroński, A. Baczmański, B. Bacroix, P. Lipinski , A. Lodini, Arch. Metall. Mater. **56**, 575-584 (2011).
[5] W. Wen, S. M.'Gull , S. Ahzi, Mater. Sci. Forum **702-703**, 241-244 (2012).
[6] W. Wen, S. M'Guil, S. Ahzi, J.J. Gracio, Int. J. Plasticity **46**, 23-36 (2013).
[7] M. Wronski, K. Wierzbanowski , T. Leffers, Mater. Sci Tech-Lond. **29**, 129-133 (2013).
[8] K. Wierzbanowski, M. Wroński, T. Leffers, Crit. Rev. Solid State **39**, 391-422 (2014).
[9] H. Hu, P.R. Sperry, P.A. Beck, J. Metals **4**, 76 (1952).
[10] F. Haessner, Z. Metallkde **54**, 98 (1963).
[11] R.E. Smallman, D. Green, Acta Metall. **12**, 145-154 (1964).
[12] I.L. Dillamore, W T. Roberts, Acta Metall. **12**, 281-293 (1964).
[13] J.S. Kallend, G.J. Davies, Phil. Mag., **25**, 471-490 (1972).
[14] P. Van Houtte, Acta Metall. **26**, 591-604 (1978).
[15] B. Bacroix, J. J. Jonas, Texture Microstruct. **8/9**, 267-311 (1988).
[16] P. Van Houtte, Acta Metall., **26**, 591-604 (1978).
[17] T.Leffers, R.K. Ray, Prog. Mater. Sci. **54**, 351-396 (2009).
[18] K. Wierzbanowski, A. Baczmanski, P. Lipinski, A. Lodini, Arch. Metall. Mater. **52**, 77-86 (2007).
[19] S. Wroński, K. Wierzbanowski, B. Bacroix, M. Wróbel, E. Rauch, F. Montheillet, M. Wroński, Arch. Metall. Mater. **54**, 89-102 (2009).
[20] W. Gambin, Plasticity and Textures, Kluwer Academic Publishers (2001).
[21] U.F. Kocks, C.N. Tome, H.R. Wenk, Texture and Anisotropy, Cambridge University Press, Cambridge (1998).
[22] M. Berveiller, A. Zaoui, J. Mech. Phys. Solids **26**, 325-344 (1979).
[23] N. Inakazu, Y. Kaneno, H. Inoue, Mat. Sci. Forum **157-162**,

715-720 (1994) .
[24] K.Z. Troost, M.H.J. Slangen, E. Gerritsen, Mat. Sci. Forum **157-162**, 1299-1304 (1994) .
[25] K. Feldmann et al., Proc. 6-th Int. Conf. on Textures of Materials, Ed. by S. Nagashima, vol. 2. pp. 1192-1200, Tokyo, Japan (1981).
[26] C.A. Bronkhorst, S.R. Kalidindi, L. Anand, Polycrystalline plasticity and the evolution of crystallographic texture in fcc metals, Phil. Trans. R. Soc. Lond. A, **341**, 443-477 (1992).
[27] H. Inoue, Y. Yoshida, N. Inakazu, Isothermal forging textures in γ-TiAl base alloys, Mat. Sci. Forum, **157-162**, 721-726 (1994).
[28] H. Schneider, P. Klimanek, Texture development in ferrous materials during deformation by pass rolling or compression, Mat. Sci. Forum **157-162**, 2037-2042 (1994).
[29] I.L. Dillamore, H. Katoh, K. Haslam, Texture **1**, 151(1974).
[30] A. Baczmański, A. Tidu, P. Lipinski, M. Humbert, K. Wierzbanowski, Mater. Sci. Forum **524-525**, 235-240 (2006).
[31] A. Baczmański, K. Wierzbanowski, J. Tarasiuk, M. Ceretti, A. Lodini, Rev. Metall-Paris **94**, 1467-1474 (1997.)
[32] A. Baczmański, N. Hfaiedh, M. François, K. Wierzbanowski, Mat. Sci. Eng. A, **501**, 153-165 (2009).
[33] K. Wierzbanowski, M. Wroński, A. Baczmanski, P. Lipinski, B. Bacroix, A. Lodini, Mater. Sci. Forum **772**, 97-101 (2014).